

## SYNTHESIS, CHARACTERIZATION, AND PHOTOCATALYTIC ACTIVITY OF $\text{Fe}_3\text{O}_4@\text{ZnO}$ NANOCOMPOSITE

Didin Sahidin Winatapura<sup>1\*</sup>, Sari Hasnah Dewi<sup>1</sup>, Wisnu Ari Adi<sup>1</sup>

<sup>1</sup> Center for Science and Technology of Advanced Materials National Nuclear Energy Agency  
Kawasan Puspiptek, Serpong, Tangerang 15314 – Indonesia

(Received: December 2015 / Revised: January 2016 / Accepted: February 2016)

### ABSTRACT

A magnetic  $\text{Fe}_3\text{O}_4@\text{ZnO}$  nanocomposite (NC) was successfully synthesized by a wet milling method using a high energy milling (HEM) machine. The magnetic  $\text{Fe}_3\text{O}_4@\text{ZnO}$  NC was characterized by an X-ray Diffractometer (XRD), scanning and transmission electron microscopes (SEM and TEM), and a vibrating sample magnetometer (VSM). X-ray diffraction results show that  $\text{Fe}_3\text{O}_4@\text{ZnO}$  NC consisted of ZnO and  $\text{Fe}_3\text{O}_4$  phases. The microstructure analysis indicated that  $\text{Fe}_3\text{O}_4@\text{ZnO}$  NC presented a ZnO shell wrapped around the surface of a magnetic  $\text{Fe}_3\text{O}_4$  surface. The average diameter of the aggregated  $\text{Fe}_3\text{O}_4$  nanoparticle (NP) is 20 nm, while that of  $\text{Fe}_3\text{O}_4@\text{ZnO}$  NCs is nearly 30 nm. The  $\text{Fe}_3\text{O}_4$  NP and  $\text{Fe}_3\text{O}_4@\text{ZnO}$  NC show typical superparamagnetic behavior with low coercivity. The saturation magnetization ( $M_s$ ) of  $\text{Fe}_3\text{O}_4$  NP was measured at about  $66.26\text{emu}\cdot\text{g}^{-1}$  and then declined to  $34.79\text{emu}\cdot\text{g}^{-1}$  after being encapsulated with a ZnO shell. The photoactivities of the  $\text{Fe}_3\text{O}_4@\text{ZnO}$  NC under UV irradiation were quantified by the degradation of a methylene blue (MB) dye solution. The result reveals that the photodegradation efficiency of  $\text{Fe}_3\text{O}_4@\text{ZnO}$  NC is favorable at pH neutral (pH = 7) reaching 100%. By increasing the MB dye concentration from 10 ppm to 40 ppm, the photodegradation efficiency decreases from 100% to 52%. The  $\text{Fe}_3\text{O}_4@\text{ZnO}$  NC can be easily collected by an external magnet. The magnetic  $\text{Fe}_3\text{O}_4@\text{ZnO}$  NC could be extended to various potential applications, such as purification processes, catalysis, separation, and photodegradation.

**Keywords:**  $\text{Fe}_3\text{O}_4@\text{ZnO}$  nanocomposite; Methylene blue; Photocatalytic activity; Photodegradation; Wet milling

### 1. INTRODUCTION

In waste water treatment technology, organic pollutants can be degraded using semiconductor photo-catalysts, such as  $\text{TiO}_2$ , ZnO,  $\text{WO}_3$ , CdS, ZnS,  $\text{SrTiO}_3$ ,  $\text{SnO}_2$ , and  $\text{Fe}_2\text{O}_3$ , with the help of UV light. Among the several semiconductor photo-catalysts used,  $\text{TiO}_2$  has been considered the most superior in terms of suitability for application. However, a ZnO photo-catalyst has been proposed as an alternative for the removal of various aqueous pollutants including organic compounds (Lee et al., 2012; Nguyen et al., 2014).

In previous studies, ZnO was used to eliminate organic pollutants such as *p-cresol*, in the reduction of metals ions, and in the degradation of Alizarine Red-S (a textiles dye) (Abdullohi et al., 2012; Liu et al., 2012; Joshi et al., 2011; Xu et al., 2014). Nonetheless, one of the main problems with the suspended photocatalyst system is that it requires a separation step to recover

---

\*Corresponding author's email: didinsw@batan.go.id, Tel. +62-21-5251109, Fax. +62-21-5251110  
Permalink/DOI: <http://dx.doi.org/10.14716/ijtech.v7i3.2952>

the photocatalyst particles. The combination of magnetic materials and a semiconductor photocatalyst could decompose hazardous organic waste water into environmentally friendly components in a more effective and simpler way. The magnetic properties in this photocatalytic system make photocatalysts very easy to be separated and recycled from wastewater after using an external magnet (Nikazar et al., 2014; Mohamed et al., 2012).

In this paper, we report the synthesis and characterization of structured  $\text{Fe}_3\text{O}_4@\text{ZnO}$  NC by a simple wet milling method. The composition of the  $\text{Fe}_3\text{O}_4$  core which was coated by a ZnO shell in the  $\text{Fe}_3\text{O}_4@\text{ZnO}$  NC was made with a weight ratio of  $\frac{1}{2}$ , and then the sample was heat treated at  $500^\circ\text{C}$  for 2 hours. Phase identification, surface morphology, elemental analysis, magnetic properties, and morphology of the particles contained in the  $\text{Fe}_3\text{O}_4@\text{ZnO}$  NC were analyzed by XRD, a SEM equipped with an energy dispersive spectrophotometer (EDS), a VSM, and a TEM. The effects of parameters such as the difference in pH and MB dye concentration were analyzed using a UV-Vis spectrophotometer.

## 2. MATERIALS AND METHODS

### 2.1. Materials

Materials which were used in the experimental procedure are reagent grade and were obtained from Merck: iron (III) chloride ( $\text{FeCl}_3 \cdot 6\text{H}_2\text{O}$ ), iron (II) chloride ( $\text{FeCl}_2 \cdot 4\text{H}_2\text{O}$ ), hydrochloric acid (HCl), zinc acetate ( $\text{Zn}(\text{CH}_3\text{COO})_2 \cdot 2\text{H}_2\text{O}$ ), sodium hydroxide (NaOH), absolute ethanol, and methylene blue (MB) dye.

### 2.2. $\text{Fe}_3\text{O}_4$ and ZnO Nanoparticles (NPs) Preparation

$\text{Fe}_3\text{O}_4$  NPs were synthesized by the precipitation of  $\text{Fe}^{+2}$  and  $\text{Fe}^{+3}$  ions with a molar ratio of 1:2 in the presence of a NaOH solution according to the method used by Winataputra et al. (2013), without modification. Briefly,  $\text{FeCl}_2 \cdot 4\text{H}_2\text{O}$  and  $\text{FeCl}_3 \cdot 6\text{H}_2\text{O}$  were prepared by dissolving them in 500 ml de-ionized water and were heated to  $70^\circ\text{C}$ . Then, a 3M-NaOH solution was added drop wise into the resulting solution under vigorous magnetic stirring. The generated black precipitations were collected by magnetic separation, washed with de-ionized water and ethanol, and dried at  $70^\circ\text{C}$ . The ZnO was obtained from zinc acetate through a co-precipitation method. The process was carried out at  $80^\circ\text{C}$  using NaOH as a precipitating agent. The white precursor was aged for 24 hours, collected, and dried in an oven at  $70^\circ\text{C}$  for 14 hours.

### 2.3. $\text{Fe}_3\text{O}_4@\text{ZnO}$ Nanocomposite (NC) Preparation

The preparation of  $\text{Fe}_3\text{O}_4@\text{ZnO}$  NC was conducted by a wet milling method using high energy milling (HEM) on a Certi-Prep 8000M machine. The formation of  $\text{Fe}_3\text{O}_4@\text{ZnO}$  NC was done in a tungsten carbide vial (Spex. 804) with a weight ratio of  $\text{Fe}_3\text{O}_4$  and a ZnO of  $\frac{1}{2}$ . The weight ratio of the precursor and tungsten carbide balls was arranged with a ratio of 1:5. The wet milling process was conducted for 10 hours, dried in an oven, and continued by the calcinations at  $500^\circ\text{C}$  for 2 hours.

Briefly,  $\text{FeCl}_2 \cdot 4\text{H}_2\text{O}$  and  $\text{FeCl}_3 \cdot 6\text{H}_2\text{O}$  were prepared by dissolving the chemicals in 500 ml de-ionized water. Then, a 3M-NaOH solution was added drop wise into the resulting solution under vigorous magnetic stirring. The generated black precipitations were collected by magnetic separation, washed with de-ionized water and ethanol, and dried at  $70^\circ\text{C}$ .

### 2.4. Characterization

The powders of  $\text{Fe}_3\text{O}_4$  NP, and  $\text{Fe}_3\text{O}_4@\text{ZnO}$  NC were characterized using an X-ray diffractometer (XRD) - Pan Analytical diffractometer, a scanning electron microscope (SEM) - JEOL JSM 6510 which was connected with an energy dispersive spectrophotometer (EDS), a transmission electron microscope (TEM) - JEOL JEM 1400, and a vibrating sample magnetometer (VSM) - Oxford 1.2T.

## 2.5. Photocatalytic Degradation

Photocatalytic degradation of the MB dye solution was performed in a water bath shaker which consisted of stainless steel housing and light from a 32 W UV-lamp located inside of the shaker. The distance from the sample to the source of the UV-lamp was about 20 cm. MB dye solutions of 10, 20, 30, and 40 ppm in concentration were used as degraded compounds. The dose used in each testing was 1g/L of MB dye solution, for 4 hours irradiation time. First, the determination of optimum pH photodegradation of the MB dye was done at pH = 3, 5, 7, 9, and 11. Then, the concentration influence of the MB dye solution was determined under UV-light illumination. The change in the concentration of MB dye solution was measured by a UV-Vis spectrophotometer (Perkin-Elmer,  $\lambda$ -25).

## 3. RESULTS

Figure 1 shows the SEM image of the dispersed Fe<sub>3</sub>O<sub>4</sub> NP and Fe<sub>3</sub>O<sub>4</sub>@ZnO NC. As observed in Figure 1a, the aggregated Fe<sub>3</sub>O<sub>4</sub> nanoparticles are ultrafine and connect tightly to one another to form groups. It is clear that some particles show a nearly spherical morphology of a rough surface, while some have regrouped to form larger aggregates. Figure 1b displays the SEM image of Fe<sub>3</sub>O<sub>4</sub>@ZnO NC. It is obvious that after being encapsulated with ZnO shell the particles show nearly spherical morphology which has a smooth surface. Comparing Figure 1a with Figure 1b, one can clearly see that the mean diameters are estimated to be about 0.1 - 0.3 nm for the Fe<sub>3</sub>O<sub>4</sub>/ZnO NC. This result indicates that the diameter of the Fe<sub>3</sub>O<sub>4</sub>/ZnO NC is a little larger than the aggregated Fe<sub>3</sub>O<sub>4</sub> particles. Figure 1c shows the energy dispersive spectrophotometer (EDS) analysis of the illuminating electron beams on the obtained Fe<sub>3</sub>O<sub>4</sub>/ZnO NC, revealing the existence of Fe, Zn, and O elements. Furthermore, the atomic present ratio of Fe to Zn elements in the spectrum is about 18: 31.92 (1/2), which is very close to the initial weight ratio of Fe<sub>3</sub>O<sub>4</sub> and ZnO, indicating the high efficiency of our method.

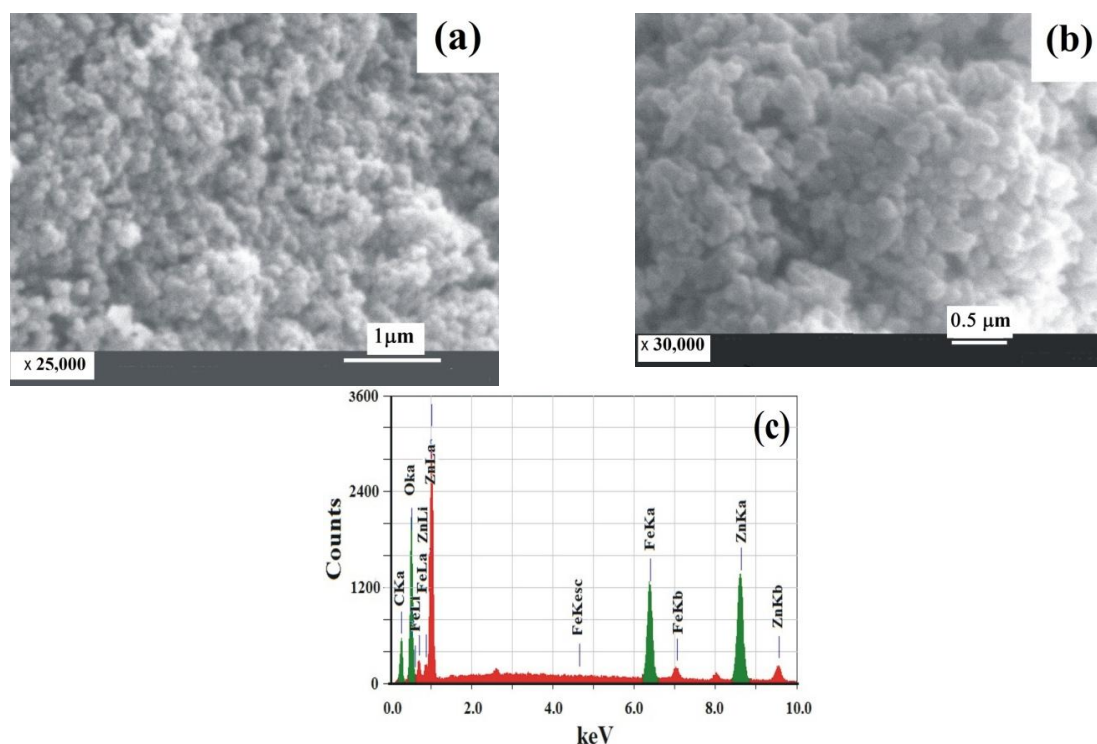


Figure 1 SEM images of (a) Fe<sub>3</sub>O<sub>4</sub> NP, (b) Fe<sub>3</sub>O<sub>4</sub>@ZnO NC, and (c) EDS spectrum of Fe<sub>3</sub>O<sub>4</sub>@ZnO NC

#### 4. DISCUSSION

Figures 2a and 2b show the X-ray diffraction patterns of  $\text{Fe}_3\text{O}_4$  NP and  $\text{Fe}_3\text{O}_4@ZnO$  NC, respectively. It can be seen that the XRD pattern of  $\text{Fe}_3\text{O}_4$  shows a single phase according to the database of JCPDS no. 19-0629 (Figure 2a). Seven diffraction peaks observed at  $18.73^\circ$ ,  $30.00^\circ$ ,  $35.50^\circ$ ,  $43.14^\circ$ ,  $53.44^\circ$ ,  $57.04^\circ$ , and  $62.58^\circ$  were well indexed to the cubic spinel structured magnetite, marked by their Miller indices (111), (220), (311), (400), (422), (511), and (440), respectively.

Figure 2(b) shows the X-ray diffraction patterns of the products after subsequent wet milling in the presence of magnetite cores. As compared with Figure 2(a), nine new non-magnetite ( $\text{Fe}_3\text{O}_4$ ) related peaks were observed at  $31.72^\circ$ ,  $34.43^\circ$ ,  $36.32^\circ$ ,  $47.53^\circ$ ,  $56.51^\circ$ ,  $62.83^\circ$ ,  $66.34^\circ$ ,  $67.91^\circ$ , and  $69.12^\circ$ . The position and relative intensity of these new peaks match well, marked by their Miller indices (100), (002), (101), (102), (110), (103), (200), (112), and (201). These peaks are attributed to the hexagonal wurtzite structure of the bulk ZnO, and accord to JCPDS card No. 36-1451. No peaks corresponding to the impurities were detected, indicating that the  $\text{Fe}_3\text{O}_4@ZnO$  heterostructure was formed during the wet milling process. This is in good agreement with the SEM/EDS analysis results described in Figure 1(c). The diffraction peaks marked with (■) indexed to the  $\text{Fe}_3\text{O}_4$  phase, while the other diffraction peaks marked with (●) are in the ZnO phase. A preferred growth orientation is along the (101) crystallographic direction. The strong sharp peaks suggest that the prepared ZnO NPs are highly crystalline. These results are in a good agreement with the results of Ahadpour et al. (2013).

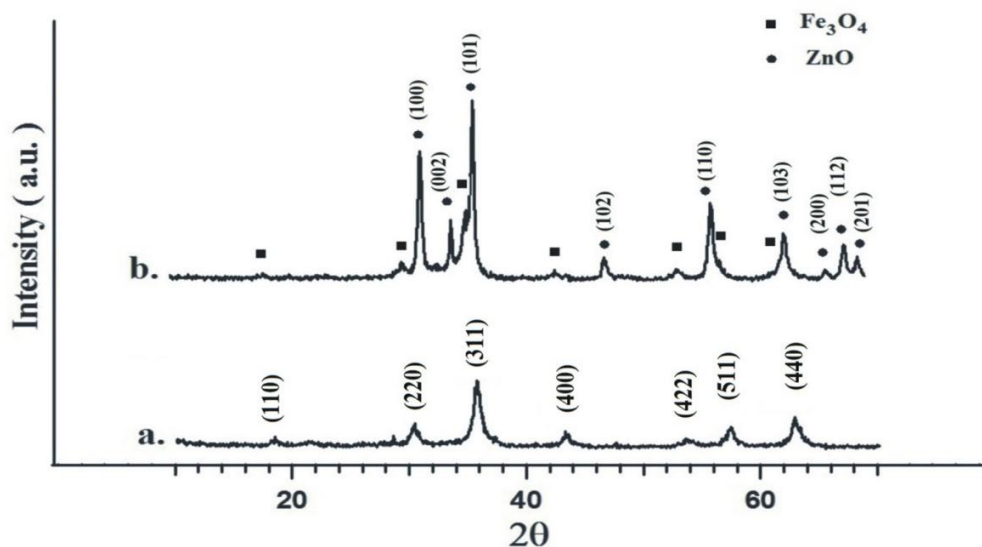


Figure 2 X-ray diffraction patterns of: (a) the  $\text{Fe}_3\text{O}_4$  nanoparticle; and (b) the  $\text{Fe}_3\text{O}_4@ZnO$  nanocomposite

The uniform and non-aggregated nature of the composite particles can be more easily recognized in TEM images, as shown in Figure 3. Figure 3 displays a TEM image of the  $\text{Fe}_3\text{O}_4@ZnO$  NC morphology prepared by a wet milling method. It can be seen that most of the  $\text{Fe}_3\text{O}_4@ZnO$  NC is nearly quasi-cubic, and has a core-shell like structure. The dark parts of  $\text{Fe}_3\text{O}_4@ZnO$  NCs are aggregated  $\text{Fe}_3\text{O}_4$  cores, encapsulated by the bright parts which are ZnO shells. The average size of the aggregated  $\text{Fe}_3\text{O}_4$  NP is about 20 nm, while the  $\text{Fe}_3\text{O}_4@ZnO$  NCs are nearly 30 nm. The electronic absorbance in the  $\text{Fe}_3\text{O}_4$  is stronger than the ZnO shell, therefore in the TEM image  $\text{Fe}_3\text{O}_4$  NPs are presented darker than the ZnO shell (Ahadpour et al., 2013). This  $\text{Fe}_3\text{O}_4@ZnO$  NC morphology exhibits a typical superparamagnetic behaviour, as measured by VSM and presented in Figure 4.

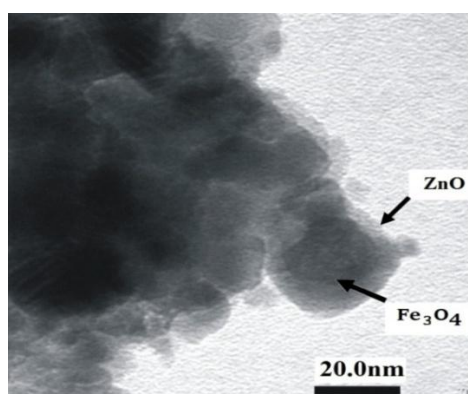


Figure 3 TEM image of a  $\text{Fe}_3\text{O}_4@\text{ZnO}$  NC synthesized by wet milling method after heat treatment at  $500^\circ\text{C}$  for 2 hours

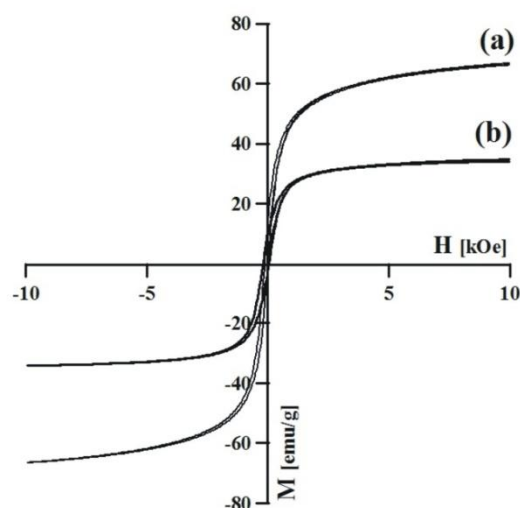


Figure 4 The room temperature  $M$ - $H$  curve of: (a) the  $\text{Fe}_3\text{O}_4$  nanoparticle; and (b) the  $\text{Fe}_3\text{O}_4@\text{ZnO}$  nanocomposite

Figure 5 represents the hysteresis curve of  $\text{Fe}_3\text{O}_4$  NP and  $\text{Fe}_3\text{O}_4@\text{ZnO}$  NC, measured by VSM at room temperature. It was found that the  $\text{Fe}_3\text{O}_4$  NP sample has typical superparamagnetic behavior and exhibits strong magnetism at room temperature with small coercivity and remanence, as seen in Figure 5a. The saturated magnetization ( $M_s$ ) of the  $\text{Fe}_3\text{O}_4$  NP sample is up to  $66.26 \text{ emu.g}^{-1}$ , which was found to be higher than that in a previous report (Winatapura et al., 2013). According to the earlier reports,  $M_s$  is  $93 \text{ emu.g}^{-1}$  for bulk  $\text{Fe}_3\text{O}_4$  materials and  $65 \text{ emu.g}^{-1}$  for  $\text{Fe}_3\text{O}_4$  NPs (Wei et al., 2011). The  $M_s$  value then decreased to  $34.79 \text{ emu.g}^{-1}$  after being encapsulated with a ZnO shell (Figure 4b). However, the  $\text{Fe}_3\text{O}_4@\text{ZnO}$  NC can be easily collected by an external magnet.

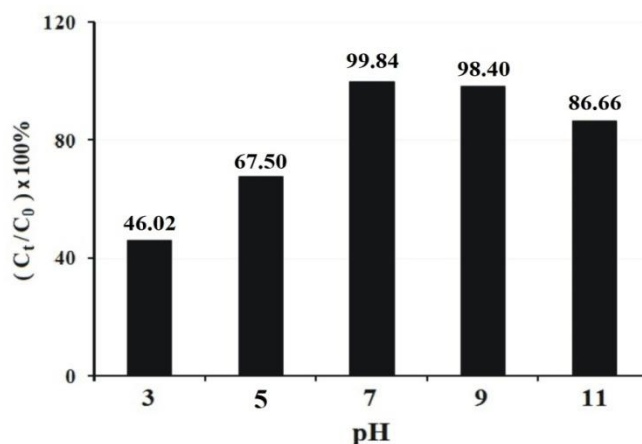


Figure 5 The photodegradation of an MB dye solution at different pH values in the presence of  $\text{Fe}_3\text{O}_4@\text{ZnO}$  NC

The  $\text{Fe}_3\text{O}_4@\text{ZnO}$  nanocomposite was used as photocatalytic to degrade the MB dye in an aqueous solution. In this work, the pH plays an important role in the photodegradation of MB dye (Abdollahi et al., 2013). Figure 5 shows the effect of pH on the photocatalytic activity of  $\text{Fe}_3\text{O}_4@\text{ZnO}$  NC. Based on Figure 5, it is seen that under an acidic condition (pH = 3) the photodegradation efficiency was unfavorable and only reached 46%. The efficiency increased significantly after increasing the pH of the dye solution to 7, and then the efficiency declined continuously to reach 86% at pH = 11. The low value of the  $\text{Fe}_3\text{O}_4@\text{ZnO}$  NC efficiency degradation is probably caused by the surface of the ZnO dissolving in acidic and alkaline conditions. The optimal pH value of the present experiment was 7. The pH effect on the photodegradation of MB in  $\text{Fe}_3\text{O}_4/\text{ZnO}$  NC can be explained on the basis of zero point charge ( $\text{pH}_{\text{zpc}}$ ), at which the surface functional groups of ZnO could be  $\text{ZnOH}_2^+$ ,  $\text{ZnOH}$ , and  $\text{ZnO}^-$  at  $\text{pH} < \text{pH}_{\text{zpc}}$ ,  $\text{pH}_{\text{zpc}}$  and  $\text{pH} > \text{pH}_{\text{zpc}}$ , respectively (Abdullohi et al., 2012; Safari et al., 2014; Vialli, 2011).

Figure 6 shows the effect of irradiation time and concentration on the photodegradation efficiency of  $\text{Fe}_3\text{O}_4@\text{ZnO}$  NC. The experiment was conducted by measuring photodegradation efficiency at different periods using 0.1 gram of  $\text{Fe}_3\text{O}_4@\text{ZnO}$  NC per 100 ml of various concentrations of dye solution (from 10 to 40 ppm). It appears that in the experiment without the particle ( $\text{Fe}_3\text{O}_4@\text{ZnO}$  NC) with UV-light, the eliminated MB dye solution of 10 ppm concentration is very low (~ 5%). This indicates that the MB dye solution only degraded by the presence of  $\text{Fe}_3\text{O}_4@\text{ZnO}$  NC with the help of UV-light.

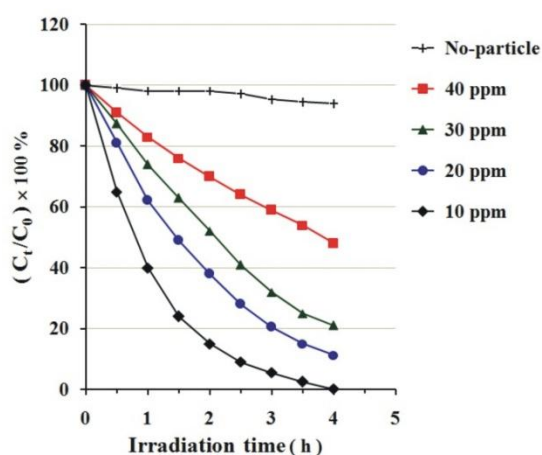


Figure 6 The photodegradation of MB dye of different concentrations without and in the presence of  $\text{Fe}_3\text{O}_4@\text{ZnO}$  NC under UV exposure

It is shown in Figure 6 that the photodegradation efficiency at MB dye of 10 ppm reached 100% degradation within 4 hours. Increasing the concentration of MB dye from 10 ppm to 40 ppm tends to decrease the efficiency of photodegradation. This means that the photodegradation efficiency of MB dye is inversely proportional to its concentration. The photodegradation efficiency value was determined and mentioned in Table 1. From Table 1, it can be clearly seen that by increasing the dye concentration from 10 ppm to 40 ppm, the photodegradation efficiency of MB dye solution decreases from 100% to 52%.

Table 1 The calculation results of efficiency, R<sup>2</sup>, and K<sub>app.</sub> values

Concentration of MB dye (ppm)	Efficiency (%)	Coefficient of determination (R <sup>2</sup> )	Photodegradation rate constant, K <sub>app.</sub> (hours <sup>-1</sup> )
10	100	0.996	0.669
20	89	0.988	0.367
30	79	0.994	0.281
40	52	0.989	0.116

The photodegradation efficiency phenomenon relates to the formation of hydroxyl (\*OH) and superoxide (\*O<sup>-</sup>) radicals that are the primary reactive species in the photocatalytic oxidation of water pollutants (Mohamed et al., 2012; Feng et al., 2014). As the concentration of MB dye solution increases, the intensity of light and illumination is fixed, so that the photons entering the MB dye solution decrease and only a few photons of the catalyst. Thus, the production of \*OH and \*O<sup>-</sup> which attack the pollutants is limited. Consequently, the relative radical numbers attached to the compound decreases and the photodegradation efficiency decreases.

The photodegradation of organic pollutants in the MB dye solution can be considered as an apparent first-order kinetic reaction (Xue et al., 2013; Xu et al., 2014) and its equation can be expressed as follows:

$$-\ln\left(\frac{C_t}{C_0}\right) = K_{app.} \times t \quad (1)$$

where K<sub>app.</sub> is the photodegradation rate constant, and C<sub>0</sub> and C<sub>t</sub> are the initial concentrations of the MB dye solution at the exposure time t. The corresponding linear plot in ln(C<sub>t</sub>/C<sub>0</sub>) as a function of irradiation time (t) is displayed in Figure 7. From Figure 7, the values of K<sub>app.</sub> and coefficient of determination (R<sup>2</sup>) can be determined, as given in Table 1. It appears that the apparent first-order kinetic equation produces a good linear graph and exhibits a coefficient of determination (R<sup>2</sup>) greater than 0.9. For a low concentration of MB dye (10 ppm), a K<sub>app.</sub> value of 0.669 hours<sup>-1</sup> can be observed, which tends to decline with the rise of MB dye concentration. This means that the reaction rate of Fe<sub>3</sub>O<sub>4</sub>@ZnO catalyst is weakened by increasing the concentration of MB dye.

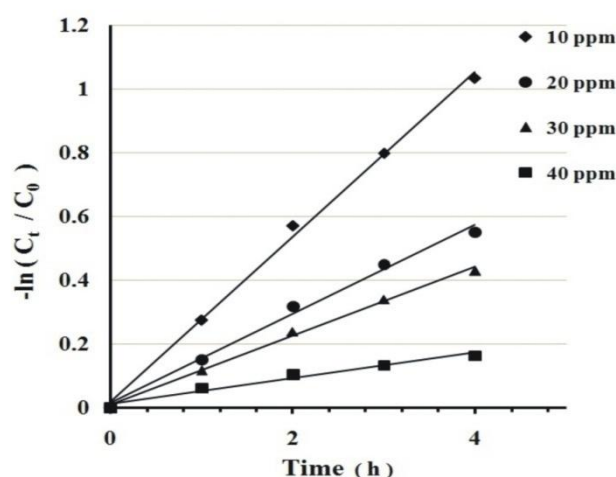


Figure 7 Apparent first order linear transforms of the disappearance of MB dye of different concentration by Fe<sub>3</sub>O<sub>4</sub>@ZnO NC under UV exposure

## 5. CONCLUSION

In this experiment, magnetic Fe<sub>3</sub>O<sub>4</sub>@ZnO NC was synthesized by a simple wet milling method. The structure, morphology, and magnetic properties of the Fe<sub>3</sub>O<sub>4</sub> and Fe<sub>3</sub>O<sub>4</sub>@ZnO samples were characterized using XRD, SEM/EDS, TEM, and VSM. The results indicate that the Fe<sub>3</sub>O<sub>4</sub>@ZnO nanocomposite consisted of Fe<sub>3</sub>O<sub>4</sub> and ZnO phases. The Fe<sub>3</sub>O<sub>4</sub> magnetic core was encapsulated by a ZnO outer shell. The aggregated Fe<sub>3</sub>O<sub>4</sub> was observed to be about 20 nm in size, while the thickness of ZnO shell was about 30 nm. The Fe<sub>3</sub>O<sub>4</sub> and Fe<sub>3</sub>O<sub>4</sub>@ZnO NC exhibit typical superparamagnetic behavior. The photodegradation efficiency optimum was reached at a neutral condition (pH = 7), and the photodegradation efficiency increased with the rise of irradiation time. By increasing the MB dye concentration from 10 to 40 ppm, the photodegradation efficiency of MB dye solution decreased from 100% to 52%.

## 6. ACKNOWLEDGEMENT

This research was supported by “Research and Development of Smart magnetic and Magnetic Oxide Programme for DIPA Grants 2015” at the Centre for Science and Technology of Advanced Materials National Nuclear Energy Agency, Republic of Indonesia.

## 7. REFERENCES

- Abdollahi Y., Abdullah A.H., Zainal Z., Yusof N.A., 2012. Photocatalytic Degradation of P-Cresol by Zinc Oxide under UV Irradiation. *Int. J. Mol. Sci.*, Volume 2012(13), pp. 302–315
- Ahadpour A., Jafari A., 2013. Study of Structural and Magnetic Properties of Superparamagnetic Fe<sub>3</sub>O<sub>4</sub>-ZnO Core-Shell Nanoparticles. *J Supercond Nov Magn.*, Volume 26 (12), pp. 1–10
- Feng X., Guo H., Patel, K., Zhou, H., Lou, X., 2014. High Performance, Recovable Fe<sub>3</sub>O<sub>4</sub>-ZnO Nanoparticles for Enhanced Photocatalytic Degradation of Phenol. *Chem. Eng. J.*, Volume 244, pp. 327–334
- Joshi K.M., Shrivastava V.S., 2011. Degradation of Alizarine Red-S (A Textiles Dye) by Photocatalysis using ZnO and TiO<sub>2</sub> as Photocatalyst. *Int. J. Environ. Sci.*, Volume 2(1), pp. 8–21

- Lee, E., Hong, J.Y., Kang, H., Jang, J., 2011. Synthesis of TiO<sub>2</sub> Nanorod-decorated Graphene Sheets and their Highly Efficient Photocatalytic Activities under Visible-light Irradiation. *J. Hazard. Mater.*, Volume 219–220, pp. 13–18
- Liu, X., Pan, L., Zhao, Q., Lu, T., Zh,u G., Chen, T., Sun, Z., Sun, C., 2012. UV-assisted Photocatalytic Synthesis of ZnO-reduced Graphene Oxide Composites with Enhanced Photocatalytic Activity in Reduction of Cr(VI). *Chem. Eng. J.*, Volume 183, pp. 238–243
- Mohamed, R.M., Mkhaliid, I.A., Baeissa, E.S., Al-Rayyani, M.A., 2012. Photocatalytic Degradation of Methylene Blue by Fe/ZnO/SiO<sub>2</sub> Nanoparticles under Visible Light. *J. Nanotechnol.*, Volume 2012, pp. 1–5
- Nikazar, M., Alizadeh, M., Lalavi, R., Rostami, M.H., 2014. The Optimum Conditions for Synthesis of Fe<sub>3</sub>O<sub>4</sub>/ZnO Core/Shell Magnetic Nanoparticles for Photodegradation of Phenol. *Iranian J. Environ. Health Sci. Eng.*, Volume 12 (21), pp. 3–6
- Nguyen, V.C., 2014. Bifunctional Core-shell Nanocomposite Mn-Doped ZnO/Fe<sub>3</sub>O<sub>4</sub> for Photodegradation of Reactive Blue 198 Dye. *Adv. Nat. Sci. Nanosci. Technol.*, Volume 5(3), pp.1–9
- Safari, M.H., Rostami, M., Alizadeh, A., Alizadehbirjandi, S.A.A., Nakhli, R., Aminzadeh, 2014. Response Surface Analysis of Photocatalytic Degradation of Methyl Tert-butyl Ether by Core/Shell Fe<sub>3</sub>O<sub>4</sub>/ZnO Nanoparticles. *J. Environ. Heal. Sci. Eng.*, Volume 12 (1), pp. 1–21
- Vialli, M., 2011. Functionalization of Zinc Oxide Nanostructures. *Ph.D. Thesis in Science and Technology of Materials Innovation*, Universita' degli studi di parma, pp. 43–45
- Winatapura, D.S., Dewi, S.H., Ridwan, 2013. Synthesis and Characterization of Fe<sub>3</sub>O<sub>4</sub>@ZnO Composite through Precipitation Method. *J. Waste Manag. Technol.*, Volume 17(1), pp. 71–77
- Wei, Y., Han, B., Hu, X., Lin, Y., Wang, X., Deng, X., 2011. Synthesis of Fe<sub>3</sub>O<sub>4</sub> Nanoparticles and Magnetic Properties. *Procedia Engineering*, Volume 27(2012), pp. 632–637
- Xue, C., Zhang, Q., Li, J., Chou, X., Zhang, W., Ye, H., Cui, Z., Dobson, P.J., 2013. High Photocatalytic Activity of Fe<sub>3</sub>O<sub>4</sub>-SiO<sub>2</sub>-TiO<sub>2</sub> Functional Particles with Core-Shell Structure. *Journal of Nanomaterials*, Volume 2013, pp. 1–8
- Xu, M., Li, C., 2014. Monodisperse Nanostructured of Fe<sub>3</sub>O<sub>4</sub>/ZnO Microrods using for Waste Water Treatment. *Adv. Powder Technol.*, Volume 25(6), pp. 1715–1720